



Empirical fragility functions and loss curves for Italian business facilities based on the 2012 Emilia-Romagna earthquake official database

Leonardo Rossi^{1,6} · Marco Stupazzini² · Davide Parisi³ · Britta Holtschoppen⁴ · Gabriella Ruggieri³ · Christoph Butenweg⁵

Received: 12 July 2019 / Accepted: 23 November 2019 / Published online: 6 December 2019
© The Author(s) 2019

Abstract

The 2012 Emilia-Romagna earthquake, that mainly struck the homonymous Italian region provoking 28 casualties and damage to thousands of structures and infrastructures, is an exceptional source of information to question, investigate, and challenge the validity of seismic fragility functions and loss curves from an empirical standpoint. Among the most recent seismic events taking place in Europe, that of Emilia-Romagna is quite likely one of the best documented, not only in terms of experienced damages, but also for what concerns occurred losses and necessary reconstruction costs. In fact, in order to manage the compensations in a fair way both to citizens and business owners, soon after the seismic sequence, the regional administrative authority started (1) collecting damage and consequence-related data, (2) evaluating information sources and (3) taking care of the cross-checking of various reports. A specific database—so-called *Sistema Informativo Gestione Europa* (SFINGE)—was devoted to damaged business activities. As a result, 7 years after the seismic events, scientists can rely on a one-of-a-kind, vast and consistent database, containing information about (among other things): (1) buildings' location and dimensions, (2) occurred structural damages, (3) experienced direct economic losses and (4) related reconstruction costs. The present work is focused on a specific data subset of SFINGE, whose elements are Long-Span-Beam buildings (mostly precast) deployed for business activities in industry, trade or agriculture. With the available set of data, empirical fragility functions, cost and loss ratio curves are elaborated, that may be included within existing Performance Based Earthquake Engineering assessment toolkits.

Keywords Empirical fragility functions · Empirical consequence curves · Precast buildings · Seismic performance of industrial facilities · Emilia-Romagna earthquake · PBEE

✉ Leonardo Rossi
rossi@lbb.rwth-aachen.de

Extended author information available on the last page of the article

1 Introduction

In assessing the seismic economic consequence on existing buildings, two complementary approaches can be adopted: on the one hand, the state of the art of PBEE (e.g. <https://peer.berkeley.edu>) provides the necessary mathematical background to rigorously define the problem from the theoretical point of view; on the other hand, field observations (e.g. Sezen and Whittaker 2006) and laboratory tests (e.g. Del Gaudio et al. 2019) allow the calibration and the validation of the developed formulas (Porter et al. 2007). As a matter of fact, the actual complexity of human activities, the usual scarcity of information and the recurrent inconsistency of data, pose serious limitations; consequently, it could be extremely challenging for all those interested to understand the on-going cause-effect correlations, to collect a significantly vast database and to create consistent datasets to be shared with other researchers. To this end, an extremely useful source of information—for what concerns business facilities—comes from recent Italian seismic events. After the 2012 Emilia-Romagna earthquake (Scognamiglio et al. 2012) indeed, the public authority of the most affected region (Emilia-Romagna) quickly set up a data collection system, to gather and process damage and consequence-related information. The aim of it was to allow a fair, well-regulated and transparent compensation process, to properly allocate public financial resources. A large part of the resulting database, so-called SFINGE (R E-R 2012b), is dedicated to buildings used for business purposes in industry, trade and agriculture. In SFINGE, there are more than 5300 different funding requests, referring to damaged, demolished, reconstructed and relocated structures (Rossi et al. 2019a). A relevant and internally consistent subset of SFINGE—with 2104 listed units—is that regarding the so-called “Long-Span-Beam” buildings (in the following, LSB); such buildings are very often single-storey, with a simple rectangular plan and prefabricated RC or metal beams between 10 and 20-m long. Vertical elements as well are, most of the times, prefabricated RC or metal-made, and just in few cases consist of normal RC or masonry. Heavy, concrete-made, simply-supported panels or masonry walls usually define the building’s perimeter. An LSB unit essentially is a business facility. The fact that the bearing capacity is mostly located in its perimeter, allows managing the internal space in a flexible way: this makes possible to use LSB buildings for a wide spectrum of activities. In this sense, this largely widespread typology can be seen as the quintessential Italian business facility. LSB structures we can read about in the Emilia-Romagna’s database were originally designed to carry almost only vertical loads, with little over-resistance and limited global ductility (see also: Liberatore et al. 2013; Magliulo et al. 2014). To this regard, it has to be noticed that, until 2003, most of Emilia-Romagna’s territory—with partial exception—was deemed “not prone to seismic hazard”; the reader can easily check this by accessing the INGV’s national seismic hazard maps, directly available at <http://zonesismiche.mi.ingv.it/>. Furthermore, a relevant evolution in terms of structural design happened in 2009, when the NTC2008 building code (MIT 2008) entered into force. This code represented a huge step forward in seismic design of structures in Italy. Nonetheless, the most part of the building stock has been built in the previous decades; for this reason, in 2012, damage and collapse often occurred because of lack of proper seismic design (Savoia et al. 2017). An example of damaged LSB building from SFINGE database, with widespread structural and non-structural damages, is reported in Fig. 1.



Fig. 1 Example of (precast) Long-Span-Beam building from SFINGE database, with widespread structural and non-structural damage. *Source:* Agenzia Regionale per la Ricostruzione—Sisma (2012)

1.1 State of the art

At the state of the art, the 2012 Emilia-Romagna sequence and its consequences were vastly described and studied in many scientific works. First of all, the Italian INGV (*Istituto Nazionale di Geofisica e Vulcanologia*) monitored and documented the entire seismic sequence, providing a series of detailed information related to the different events (e.g.: source inversion, shakemaps, etc.). Events' shakemaps are publicly available on the official websites of both INGV (2012) and United States Geological Survey (2012). Further documentation about the sequence, including reconnaissance photos, is reported in a dedicated clearinghouse—run by Earthquake Engineering Research Institute (EERI)—available at <http://learningfromearthquakes.org>. In Lauciani et al. (2012) and Cultrera et al. (2014), the shakemaps of the sequence events are reported, and their inherent uncertainties are appraised and discussed. To be noticed that, during the Emilia seismic sequence, at the time of the emergency management, shakemaps have been adopted as a benchmark for decision making regarding the safety checks to be implemented (see again Cultrera et al. 2014). After the shock of May 20th (M_w 5.86, Scognamiglio et al. 2012), the network of recording stations impressively widened: at least 60 devices were installed by the INGV and other institutes in the immediate aftermath of the event. Then, two major shocks, of magnitude M_w 5.66 (Scognamiglio et al. 2012) and 4.7 (INGV 2014), were recorded on May 29th and June 3rd respectively. During the entire seismic sequence and soon after it, field observations were conducted both by public officials and scientific teams; reports can be found in Rossetto et al. (2012), Parisi et al. (2012), D'Aniello and La Manna Ambrosino (2012). Structural performance of precast RC industrial buildings was discussed in Savoia et al. (2012), Liberatore et al. (2013), Magliulo et al. (2014), Belleri et al. (2015), Nascimbene et al. (2015), Minghini et al. (2016), Savoia et al. (2017). Precast industrial buildings have been the topic of guidelines regarding structural typology definition—before

(Bonfanti et al. 2008; Toniolo and Colombo 2012) and after the earthquake (Bellotti et al. 2014)—as well as seismic improvement interventions methodologies (GLASCI 2012), the latter being mainly focused on creating and strengthening links between precast elements. The whole set of acts of law, administrative decrees and technical guidelines released by Regione Emilia-Romagna can be found on <https://www.regione.emilia-romagna.it> and is summarised in Pres. R E-R (2012a, b). A preliminary economic analysis of the reconstruction of the affected businesses was described in ARR (2018) and R E-R (2018), while an introduction to SFINGE and first data analysis results were reported in Rossi et al. (2019a, b). A first contribution regarding the empirical seismic fragility curves for precast RC structures from 2012 Emilia evidences was given in Buratti et al. (2017); in this case, the information is mostly coming from field surveys. On the contrary, in the following, fragility and loss curves are obtained from SFINGE's data: this means that the here adopted information went through the entire Emilia-Romagna's internal procedure for data cross-checking and validation (see Rossi et al. 2019a). Additionally, in this work, relevant economic aspects are considered among the seismic consequences. This work is intended as a contribution to the field of PBEE and to its existing reference frameworks (e.g.: ATC 2012; GEM Foundation 2018) and works (Syner-G Consortium 2013; Miranda and Aslani 2003; Aslani 2005).

1.2 SFINGE's LSB subset

For the 2104 LSB structures listed in SFINGE database, among the many information available, it was possible to directly access the following record fields: (1) geographical position (with a subsequent great potential in terms of correlation with site effects and information about the ground characteristics), (2) total area, (3) structural damage, (4) content damage, (5) parametric loss, and (6) cost of interventions. It has to be noticed that the structural damage occurred to individual buildings was described through technical reports and then briefly summarized by means of a six-grade damage scale, hereafter described in terms of damage patterns (see also Pres. R E-R 2012b; Rossi et al. 2019b):

- *P1* no collapse (neither global nor local). Local or widespread light damage on vertical and/or horizontal structural elements, on up to 20% of total elements' surface. Building's operativity can be recovered with local strengthening interventions (LSI). Such local interventions may be followed by seismic improvement interventions (SII), to meet the safety requirements imposed by law in the affected area.
- *P2* no collapse (neither global nor local). Widespread light damage to vertical and/or horizontal structural elements on at least 20% of total elements' surface. Building's operativity can be recovered with LSI. Such local interventions may be followed by SII.
- *P3* serious structural damage, with collapse on up to 15% of vertical and/or horizontal structural surfaces. And/or damage to one or more beam-column joints, with relative permanent displacement greater than 2% of column's height. And/or relevant absolute settlement of the footings—i.e. greater than 10 cm and lower than 20 cm. And/or relevant relative settlement of the footings—i.e. greater than 0.3% of L and lower than 0.5% of L, with L = distance between the columns. Building's operativity requires SII.
- *P4* extremely serious structural damage, with partial collapse, on up to 30% of vertical and/or horizontal structural surfaces. And/or damage to up to 20% of beam-column joints, with relative permanent displacement of more than 2% of column's height. And/or plastic hinges at the base of up to 20% of the columns. And/or rel-

Table 1 Number of buildings by damage pattern

Damage pattern	P1	P2 ^a	P3	P4	P5	P6	Total
Number of buildings	1042	434	180	139	288	21	2104

^aIn two cases, information about reconstruction cost is not available

Fig. 2 Example of damage patterns P1–P2. *Image source:* Agenzia Regionale per la Ricostruzione—Sisma (2012)



evant absolute settlement of the footings—i.e. greater than 20 cm. And/or relevant relative settlement of the footings—i.e. greater than 0.5% of L, with L = distance between the columns. Building's operativity requires SII.

- P5 building collapsed or so highly damaged (i.e. worse than damage pattern P4) that it has to be demolished.
- P6 damage pattern that can't be described by one of the five previously listed. This pattern regards non-building structures (e.g. water tanks); it can be considered irrelevant to the aim of this paper and will be mostly disregarded in the following.

For the reported scale, relevant similarities exist with the damage classification of the European Macroseismic Scale—EMS98 (Grünthal 1998). Table 1 summarizes the number of buildings by experienced damage pattern.

Damage patterns P1 and P2 can be considered similar to each other, and referred to in terms of *light-moderate* damage; an example of such consequence level is given in Fig. 2, where the reader can see cracks appearing between the structural elements, and a false ceiling being partially collapsed. Levels P3 and P4 can be seen as close each other too, and referred to as *serious* damage; an example is given in Fig. 3, where a heavily damaged precast beam-column joint is depicted. As emerges from the description of the

Fig. 3 Example of damage patterns P3–P4. *Image source:* Agenzia Regionale per la Ricostruzione—Sisma (2012)



damage pattern we reported above, the relative number of actually affected structural elements determines the classification pattern.

Finally, a P5 damage pattern is depicted in Fig. 4: the reader can see that a precast joint collapsed and that the hosted beam fell down to an underlying support; a red arrow, between two straight lines parallel to the ground, highlights the element's vertical dislocation.

Accessing the data on the LSB-dataset, the average cost of structural works for each damage pattern can be obtained. For the way the patterns were defined, when it comes



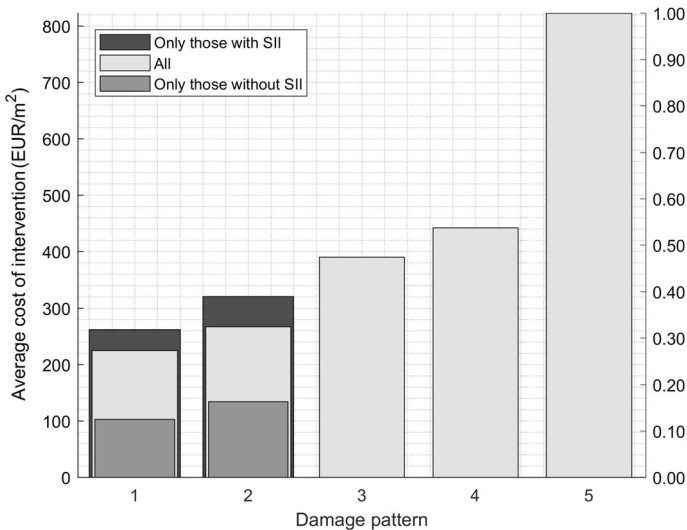
Fig. 4 Example of damage pattern P5—detail of a collapsed precast beam-column joint. *Image source:* Agenzia Regionale per la Ricostruzione—Sisma (2012)

Table 2 Cost of works by damage pattern

Damage pattern	P1	P1 ^a	P1 ^b	P2	P2 ^a	P2 ^b	P3	P4	P5
Number of items	1042	239	803	432	125	307	180	139	288
Average of listed unitary cost of works (€/m ²)	225	103	262	267	134	321	390	442	823

^aConsidering only those cases without SII

^bConsidering only those cases with SII

**Fig. 5** Graphic representation of data of Table 2

to P1 and P2, repairing actions could also be followed by additional seismic improvement interventions (SII); the scope of such interventions was to enhance the building's seismic capacity to at least 60% of what the then in-force Italian building code (MIT 2008) recommended for new structures; as the reader can imagine, this affects the final cost of works. In Table 2 we report the number of items and the average of unitary cost of works, by damage pattern [in Rossi et al. (2019b), a paper written at a stage when data were less disaggregated, the authors instead provided values of total cost divided by total area for every subset].

From Table 2 (see also the graphic representation in Fig. 5), it should be noticed that damage pattern P5 is associated with a much larger average unitary cost than P4: when considerable structural collapses occur, the complete reconstruction of the building is the only option and therefore the unitary cost of the intervention is much larger than in the other cases. More details about the values shown in Table 2 can be found in ARR (2018) and Rossi et al. (2019b).

From Fig. 5 it clearly emerges as, when SII are not included, the first two levels of damage are much cheaper than the others (indeed they can be considered as *light damage*). On the contrary, when additional interventions are put in place, even light damage

may have a considerable unitary reconstruction cost (i.e. not so far from those of damage patterns P3 and P4).

2 Empirical evidences representation

As previously mentioned, the area affected by severe ground motion during the 2012 earthquake sequence was relatively well constrained—being within a 50 km range (Scognamiglio et al. 2012)—especially in the aftermath of the 20th of May event. Nonetheless, until June 6th 2012, tens of relevant shocks contributed in generating or extending structural and non-structural damage. So, in order to be able to effectively put in relation recorded seismic intensity with observed consequences, we deemed necessary to take into consideration multiple events of the 2012 sequence. As work’s first step, it was decided to collect from the INGV’s archive (<http://shakemap.rm.ingv.it/>) 45 data files, i.e. all those regarding Emilia-Romagna’s events with a moment magnitude equal or greater than 4.0, and then to summarise the available information in an “enveloped shakemap”: in such a map, at each location, only the maximum value of ground motion among all the events, was considered. Results of the envelopment are reported in Fig. 6: on the left-hand side the Peak Ground Acceleration (PGA) is presented, while the Mercalli Modified Intensity (MMI)—(Wood and Neumann 1931)—is visible on the right-hand side. In both cases, black triangles represent the recording stations that were active on May 29th 2012 (Paolucci et al. 2015), while blue stars—whose size is proportional to the corresponding recorded magnitude—display the epicenters of the considered events.

The two aforementioned maps present quite different shapes: in a nutshell, the one about MMI seems to be much more radially symmetric than the one regarding PGA. The reason for this could be the following: on one hand, MMI values are based on damage levels—provoked by the seismic sequence—that were evaluated ex-post; thus, the contributions of all the occurred shocks are in some way piled up. On the other hand, PGA values are obtained by events recording, and thus they are conditioned by the actual number and quality of active stations.

In Fig. 7, a scatterplot of the damage patterns data points, as available in SFINGE, is superimposed to the previously mentioned sequence envelopment maps—it should be

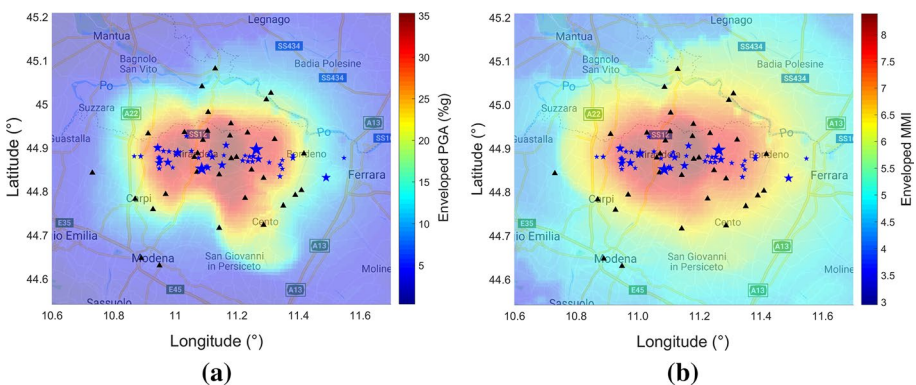


Fig. 6 Envelopment of the Emilia-Romagna sequence’s main shakemaps, in terms of **a** Peak Ground Acceleration (PGA) (%) and **b** Mercalli Modified Intensity (MMI)

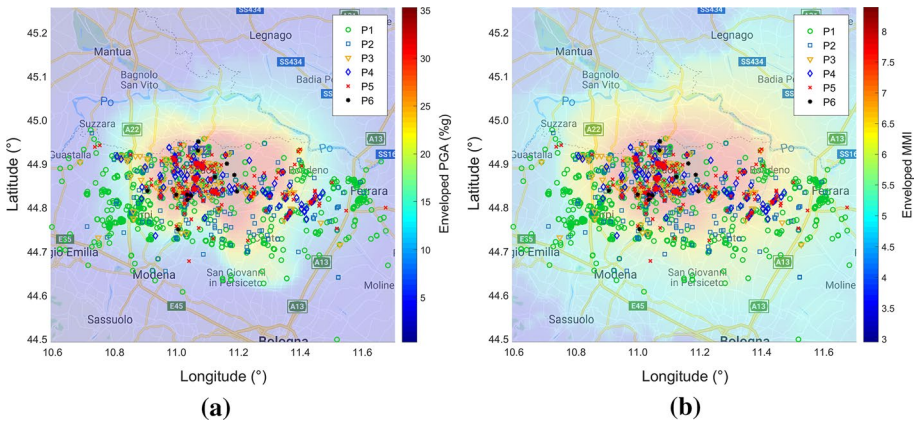


Fig. 7 Damage pattern scatterplots superimposed to sequence envelopment shakemaps. **a** Peak Ground Acceleration (PGA) (%g) and **b** Mercalli Modified Intensity (MMI)

highlighted that the maps are available thanks to the fact that each LSB-item was characterized by geographical coordinates. In Fig. 7, different damage patterns on LSB-structures are represented with different colours and symbols. On one hand, the figure proves that the density of reported damage items is significantly higher in the reddish area—as expected—being it clearly related to the highest intensity of shaking; on the other hand, few buildings got serious structural damage in the blue zone (low intensity).

Presented information can be put on a different space: in Fig. 8, we report the normalised cumulative amount of damaged buildings—by damage pattern—as a function of PGA. The reader can see how P1-items are almost linearly distributed along the horizontal axes. On the contrary, the other damage patterns present a much steeper trend for PGA values between 28% and 35% of g, i.e. they are mostly activated at higher intensities of shaking [It should be mentioned that—taking as a reference the town of Mirandola, and an amplification factor S of 1.48—a PGA value of 0.28 g is above the

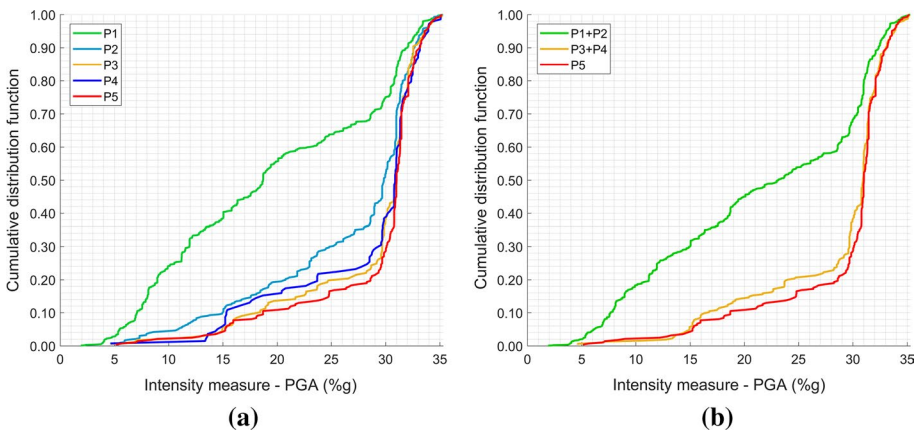


Fig. 8 Cumulative distribution functions of damaged items versus ground motion intensity (PGA, as % of g) with **a** five damage patterns and **b** three damage patterns

expected one for a return period of 475 years (MIT 2008, 2018)]. In Fig. 8a, it can also be observed that P4 curve lays above P3 curve: at first sight, this could look partially counter-intuitive. One could expect that, in a set of buildings with the same structural capacity, a damage condition P_i may never happen before P_{i-1} . The trends of the curves of Fig. 8 can be explained with three considerations: (1) in the empirical dataset we have, made of real buildings, any two items will never have the very same structural capacity. (2) We adopted the max value of experienced PGA, as a reference intensity measure parameter; but such parameter can't completely describe the history of seismic demand during an event, nor can provide information about the entire sequence of shocks actually occurred. Regarding the latter aspect, in some cases, the manifestation of tens of medium intensity shocks may, in theory, have provoked a structural damage equal or greater as in those sites where acceleration had its peak. (3) As already discussed in this text, for the way they are defined, similarities emerge among damage patterns; this means that the fact that curves P3 and P4 cross each other is not extremely relevant.

By considering P1 and P2 values as belonging to one single subset, and by doing the same with P3 and P4 items, we get what is reported in Fig. 8b. Here, cumulative curves already plotted in Fig. 8a (except P5) are reshaped, as the normalised distributions of number of buildings by PGA change. Nonetheless, P1 and P2 together tend to have a pseudo-linear trend, while both P3 and P4 together still present the late-step already plotted in Fig. 8a.

Similarly to Fig. 8, damage information can be plotted by Peak Ground Velocity (PGV) as well, and this is shown in Fig. 9. The same considerations made for Fig. 8, regarding curves crossing each other, stay valid.

From Fig. 9 it can be noticed that, in comparison to PGA-based charts, those PGV-based are more uniformly distributed all along the X axis.

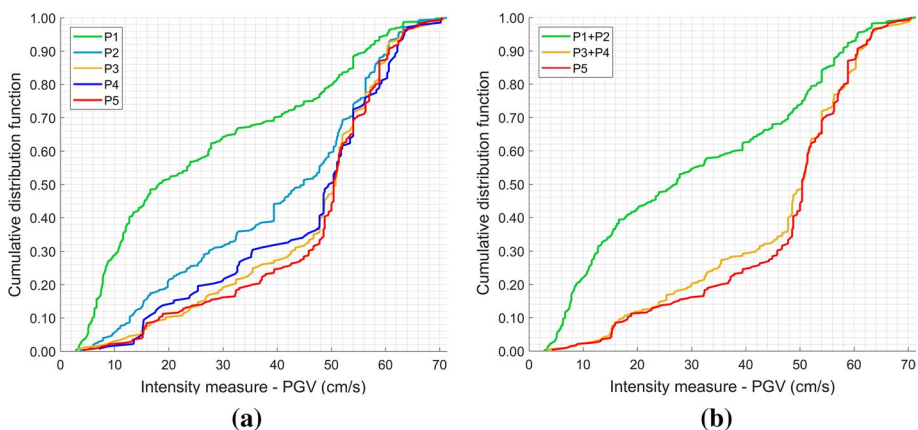


Fig. 9 Cumulative distribution functions of damaged items versus ground motion intensity (PGV, in cm/s) with **a** five damage patterns and **b** three damage patterns

3 Fragility empirical evidence

As a further step of data representation, from the reported charts of Figs. 8 and 9, by counting the relative number of items per damage pattern, per intensity measure bin, it is easy to get the corresponding fragility empirical bar plots that are shown in Fig. 10. These can be considered as first approximations of empirical fragility curves, respectively in terms of PGA and PGV. Actually, they provide the conditional probability of incurring into a certain damage pattern— P_i —as a function of the intensity measure bin. The term “conditional” is used here, as we are considering the case for which a certain non-zero damage pattern (DP) has occurred (see Formula 1).

$$\mathcal{P}(DP = P_i | DP \neq P_0) \tag{1}$$

In the formula, subscript i takes values from the set $\{1, 2, 3, 4, 5\}$, and P_0 represents the undamaged state. In the following, we will discuss about how to assess the probability $\mathcal{P}(DP \neq P_0)$, so to reshape the chart and make it *unconditional*.

For the charts of Fig. 10, as a first attempt, the number of bins on the X-axis was set equal to 7—this produces a PGA span of circa 5.0% g and a PGV span of 10.2 cm/s respectively. Looking at the figure, it is easy to notice that the trends within the bar stacks are not fully monotonic, differently from what can be expected as a basic requisite of such kind of charts; indeed, being the plots data-based, when keeping the bins’ span fix, the number of data points per intensity-measure-bin can be considered as a random variable. This is due to the fact that neither the ground motion values nor the buildings are uniformly distributed within the territory; in Emilia-Romagna, industrial structures tend to be clustered in relatively small “industrial areas”, while the ground motion intensities are roughly concentrically distributed, with the highest values within a small central zone and the lowest ones in vast peripheral areas; obviously, bins characterized by a smaller number of data points can easily experience a large internal variability. Another aspect to be considered is that, even if LSB structures are similar to each other in terms of design principles, scope and, consequently, structural features, they are not characterised by an identical *demand/capacity ratio* (DCR). In other words, a set of non-uniformly distributed buildings, with different DCR, experienced different ground motion time histories. One limitation of the bar plots of Fig. 10 is that they do not show the minimum value of the intensity measure at which the

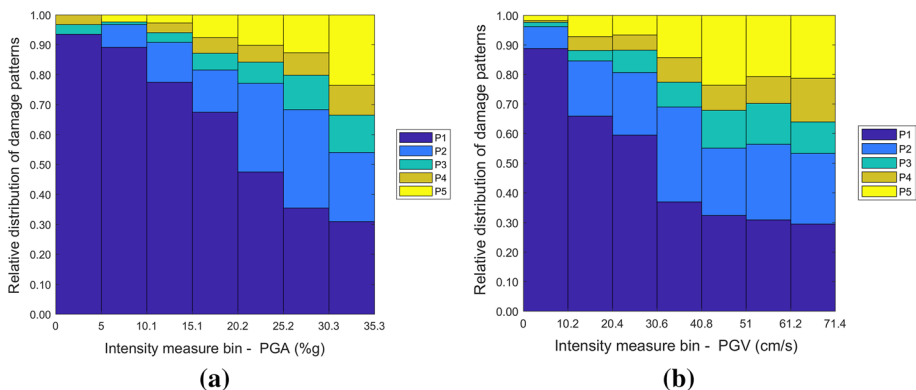


Fig. 10 LSB buildings empirical fragility curves by **a** PGA (as % of g) and **b** PGV (in cm/s)

damage actually occurred (on the other hand, what we do know is that the recorded input was not strong enough to activate worse damage states); this is due to the fact that PGA and PGV were obtained without taking memory of the corresponding damage progression. As a consequence, such shortcoming may lead to an overall overestimation of the actual structural capacity. Despite the limitations, the reported bar plots provide the reader with useful information about the fraction of LSB buildings he/she can expect at every intensity measure bin. Finally, the reader interested in considering aggregated damage patterns P1 + P2 and P3 + P4, can simply refer to the reported charts, just adding together the corresponding stacks.

In literature, relevant works on fragility curves obtained from empirical data exist—(e.g. D’Ayala et al. 1997; Sabetta et al. 1998; Yamaguchi and Yamazaki 2000; Rota et al. 2008; Rossetto et al. 2013; Casotto et al. 2015; Lin et al. 2016; Buratti et al. 2017; Hofer et al. 2018); in Buratti et al. (2017) in particular, the focus is on the same seismic events here considered—Emilia-Romagna 2012—and on a comparable building stock; in such relevant work, the number of structural units is 1890, of which 967 suffered no damage during the seismic sequence. The remaining ones—923—were classified according to the hereby reported 5 damage patterns. The database we used in this work can be considered an extension of Buratti’s, not only in terms of number of items, but also for what concerns both data fields—we accessed files regarding economic aspects too—and information reliability; a comparison of the two data sources can be found in Rossi et al. (2019b).

4 Parametric loss and reconstruction cost data representation

In the LSB dataset, the amounts of direct economic losses are reported for each of the listed buildings; in particular, such amounts exclusively regard real estate items (i.e. contents and business interruption are not taken into consideration), and for this reason they could be named “*Direct Real-estate-related Economic Losses*”—see also (Rossi et al. 2019b); for brevity, here we indicate them with the Greek letter “ Θ ”. Every Θ value was computed by technicians delegated by the business owners during the funding application phase, and was determined by multiplying the affected area by a parametric unitary loss, the latter depending both on the experienced damage pattern (P1–P5) and on building’s typology (Pres. R E-R 2012a). The obtained value represents a parametric reference amount, assumed to be the maximum refunding sum that can be demanded to the public authority (see Rossi et al. 2019b). From Θ values, dividing each entry by the corresponding building total area, we get the so-called “ θ ”; this second entity is more portable than the previous one, as it can be considered independent from buildings’ area. A second relevant variable in LSB dataset is *Direct Real-estate-related Economic Cost* (here referred to as Γ). The Γ values were reported by applicants asking for refunding, and represent the amount of money actually spent for the reparation, retrofitting and/or reconstruction of buildings (depending on the damage pattern). In particular, Γ includes all the necessary costs for structural components, structure-related finishings and systems, technical and safety services, and the necessary tests on materials and structural elements (see also Rossi et al. 2019b). Γ items were evaluated considering reference unitary price lists—(R E-R 2012a; R E-R 2013)—and actual material and work quantities. In a nutshell, with regards to the reconstruction works, θ is computed ex-ante, while Γ is obtained ex-post. Again, γ values were derived by considering the respective building area. Figure 11 shows the cumulative distribution functions (CDF) of Log10 of both θ and γ ; in it, corresponding theoretical

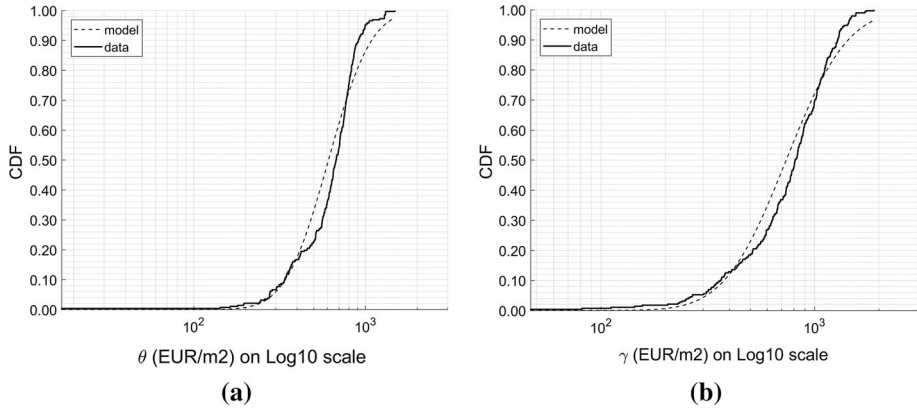


Fig. 11 Cumulative distribution functions for **a** θ and **b** γ —see also (Rossi et al. 2019b)

distributions are also depicted, and the reader can notice a certain similarity to the lognormal behaviour. Interestingly, the data points of both θ and γ can be plotted over the seismic sequence envelopment map, as shown in Fig. 12: circles have a diameter proportional to the Log10 of the corresponding amount (in EUR/m²), and an edge colour depending on the damage pattern. Once again, items representing serious damage are far more frequent in the reddish area.

Finally, in Fig. 13 we report the θ – γ scatterplot, so to show the correspondence between the two entities; the reader can also see the dashed parity line—i.e. $y=x$ (in red). As highlighted by (ARR 2018), there is always a positive correlation between θ and γ values, for every considered damage pattern—see Table 3; the correlation is closer to one for the last two, more serious, damage levels; this means that the parametric losses (assessed ex-ante) tend to be closer to the actually spent (ex-post) amount of money as damage worsens. Because of that, the parametric loss assessment proposed by Regione Emilia-Romagna (Pres. R E-R 2012b) can be considered a reasonable first-order approximation of reconstruction costs in LSB-type buildings, and may be used in the future. What the ex-ante

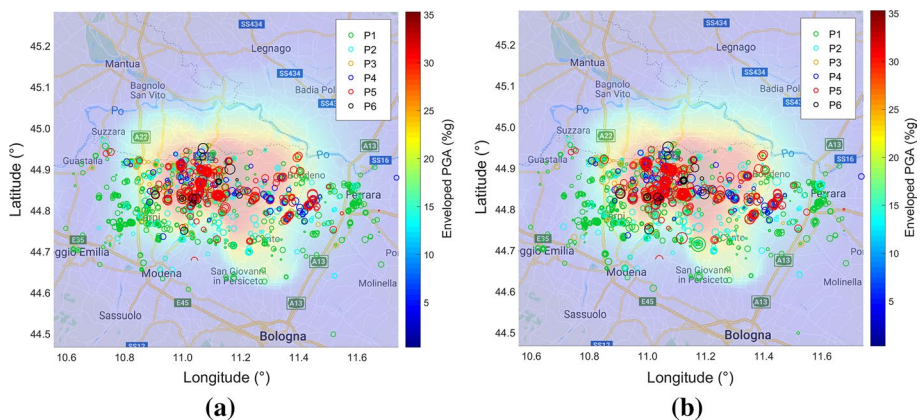


Fig. 12 Direct economic consequence superimposed to an envelopment shakemap (in terms of PGA—as % of g). **a** On the left-hand side, values of θ and **b** on the right-hand side, values of γ

Fig. 13 θ – γ scatterplot (Log10)

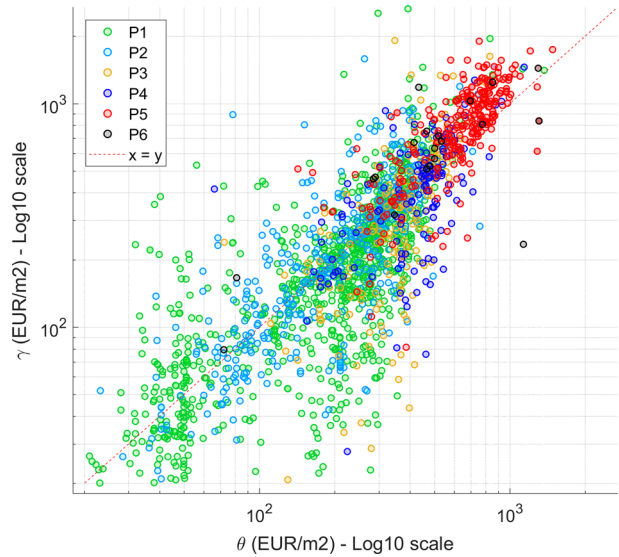


Table 3 Correlation coefficients between θ and γ , for different damage patterns

Damage pattern	P1	P2	P3	P4	P5	All ^a
θ – γ correlation coefficient	0.84	0.86	0.84	0.97	0.95	0.89

^aExcluding P6

evaluation is not able to describe, is the possible existence of both insurance policies and additional private investments, that can make the reconstruction cost—for the way it was defined here—significantly larger than the parametric loss. Furthermore, from Fig. 13 we notice that the worse the damage pattern, the less widespread the data points. For example, P1 values have a large dispersion and many times they lay far from the parity line. On the other hand, P5 points are close each other, mostly in the upper-right region and not far from the red dashed line. Again, we interpret this as an indication that light damage is more difficult to assess both in terms of parametric losses θ and actual reconstruction costs γ .

4.1 Cost curves characterisation

As a further investigation step, it is possible to make use of the information record regarding the buildings’ geographical position, and to combine it with the Γ values. To this regard, for every point on the maps of Fig. 7, we consider the minimum distance from the two biggest events’ epicenters, δ ; this makes possible to plot a δ versus cumulative- Γ chart, as shown in Fig. 14. As the reader can see, circa 95% of Γ was generated for $\delta \leq 30$ km (a detail is shown in Fig. 14b). Furthermore, 50% of total Γ belongs to $\delta \leq 7.5$ km. In other words, this means that, for what concerns LSB structures, the 2012 Emilia-Romagna sequence provoked most of the direct—real estate-related—economic consequences in the near fault region.

Given that the position of LSB buildings in the database is known, and considering the enveloped shakemaps—both in terms of PGA and PGV—it is possible to plot the

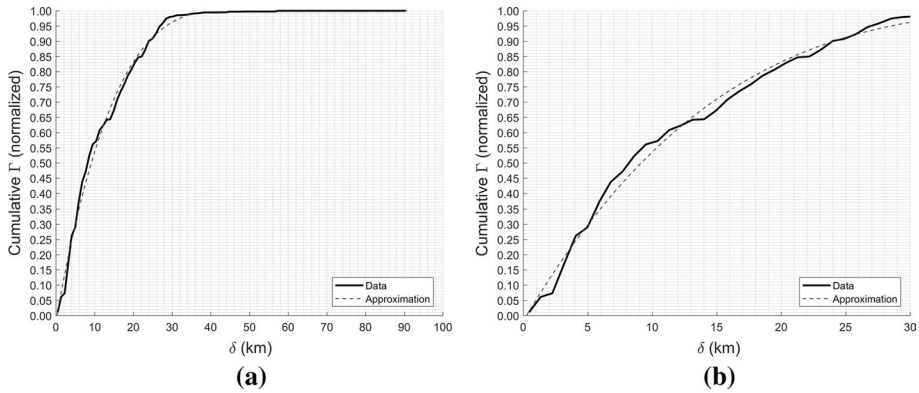


Fig. 14 δ versus cumulative- Γ plot; **a** whole picture **b** detail, with $\delta \leq 30$ km

cumulative function of Γ in terms of intensity measure (IM). Results are shown in Fig. 15, where red dashed lines indicate quartiles.

For what concerns the PGA-plot (Fig. 15a), we see an initial almost-linear trend, then a steep increase at around 28% of g , so that 50% of the Γ items belong to the narrow range beyond that value. On the contrary, when it comes to PGV (Fig. 15b), the cumulative distributions are closer to linearity—the median being at circa 38 cm/s. It is worth remembering that many buildings belonging to the studied set were characterised by poor beam-column connection; often, no metal dowel is put between the two elements, and the joint relies just on friction. From this point of view, the idea of a critical level for the horizontal acceleration, above which the friction alone can't guarantee connection anymore, is not in contrast with what is shown in Fig. 15a. On the other hand, the PGA chart is probably influenced by a saturation effect in recording the acceleration values: this would make the curve looking steeper than it is in reality. Further investigation (including, for example, ground motion simulation) is needed in this sense. Nonetheless, provided charts of Fig. 15 can be used in seismic loss assessment, when evaluating the expected relative amount of Γ by ground shaking intensity range. To this regard, other limitations have to be taken into

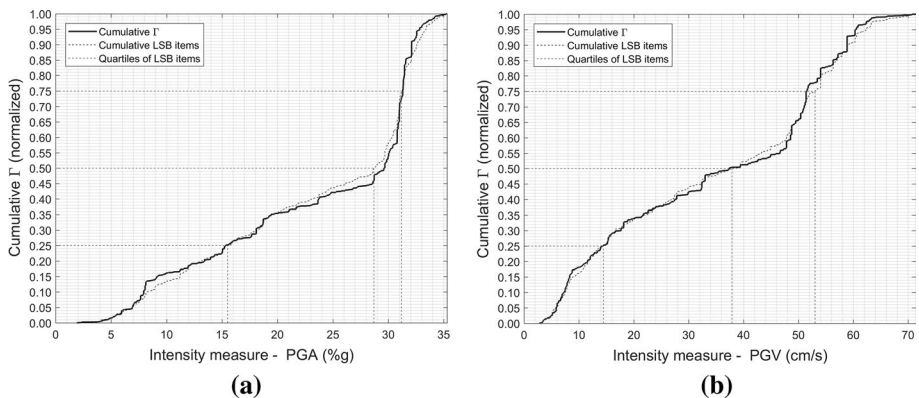


Fig. 15 IM versus cumulative Γ plot, with abscissa in terms of **a** PGA (%g) and **b** PGV (cm/s)

consideration: on one hand, results depend on the specific seismic scenario of 2012 Emilia-Romagna earthquake, i.e. not only on the characteristics of the occurred shocks, but also on the geographical distribution of LSB buildings (and their structural capacity), and on the socio-economic context of the region. On the other hand, in this study we ignored the vertical component of the acceleration, that may play a role in reducing the joint's horizontal capacity (Liberatore et al. 2013; Bovo and Savoia 2019). Nonetheless, the reported information represents a first reference for possible comparable events in Italy, and in particular in seismic prone regions with similar building stocks (e.g. Umbria, Marche and Veneto).

4.2 Assessed real-estate total values and loss ratios

One way to enhance the portability of available information about Γ , is to transform it into a *loss ratio*, i.e. the ratio between the building's reported reconstruction cost and the initial real estate total value. Given that in our LSB dataset there is no explicit entry about the latter, in this work we had to assess it, obtaining a variable that we called "*Assessed Real Estate Total Value*", or " Ψ " (see Formula 2).

$$\Psi_i = \omega \cdot A_i \quad (2)$$

In Formula 2, A_i is the area of the i th building, while ω is an assessed unitary construction cost for an LSB structure (in EUR/m²). In theory, many different approaches were possible to determine ω ; in practical terms, we took the mean of γ values for buildings that experienced a damage pattern equal to P5 (see Formula 3, where N is the number of considered items).

$$\omega = \frac{\sum_{j \in P5} \gamma_j}{N} \quad (3)$$

Once Ψ_i is known, the *assessed loss ratio* ξ can be calculated as in Formula 4.

$$\xi_i = \frac{\Gamma_i}{\Psi_i} = \frac{\gamma_i}{\omega} \quad (4)$$

In the database there are 288 structures (13.7% of total) experiencing a damage pattern of level 5; as already shown in Table 2, from them we get an ω equal to 823 €/m². It has to be noticed that the obtained value includes the amount of money spent for: (1) rubble removal; (2) necessary demolitions; (3) technical costs; (4) tests on materials and components. Interestingly, ω can be disaggregated by business macrosector (industry, trade and agriculture), thus obtaining what reported in Table 4. From the table, we see how the largest values of both ω and Ψ are obtained for industrial activities, while the smallest ones

Table 4 ω values by business sector

Business macro-sector	Industry	Trade	Agriculture	Total
No. of P5 buildings	185	18	85	288
ω (EUR/m ²)	928	909	576	823
Total Ψ (EUR)	2.61×10^9	4.89×10^8	3.55×10^8	3.45×10^9
Total ξ (%)	34.9	24.7	54.0	35.4

belong to agriculture. Despite that, agriculture had the largest total loss ratio. Obtained results are integrated in what is presented in the following sections.

5 P0-tower assessment

For the way it was assembled, LSB dataset does not contain any direct information about non-damaged buildings (hereafter so-called “P0”, or *pattern zero*, items). Nonetheless, in order to develop consequence curves and fragility functions, the amount of P0 elements had to be estimated. Within the considered regional area, damaged LSB buildings were reported to the public authority in 54 different towns; for such towns we determined the number of non-damaged items.

First of all, it has to be considered that, if not included in the dataset we investigated, an LSB building can be classified according to one or more of the following cases (see also Rossi et al. 2019b):

- Damage and loss didn’t occur to real-estate but rather to content (products and/or machineries); in this case, building’s data were also collected in SFINGE, but they are not included in the LSB dataset—see Rossi et al. (2019b).
- The insurance policy paid full compensation for the suffered loss (the rate of insurance penetration within the area is assessed to be in the order of 10%, see Rossi et al. 2019a).
- No public financial aid was asked for losses not covered by the insurance (e.g. deductibles). Apparently, this could be the case of relatively small losses.
- Funding application was rejected by Emilia-Romagna or quitted by the applicant; this is the case for applications where the information provided is wrong and/or false and/or insufficient.

Trivially, the total number of undamaged LSB structures within the 54 town is given by Formula 5.

$$P0 = \sum_{k=1}^{54} P0_k \quad (5)$$

In Formula 5, “k” indicates the generic town for which we have data, and $P0_k$ is the difference between the thereby total number of LSB buildings (T_k), and the corresponding amount of damaged items actually reported in the LSB-dataset (R_k)—see Formula 6.

$$P0_k = T_k - R_k \quad (6)$$

In order to assess the values of $P0_k$, we used an empirical curve reporting the density of LSB structures by town population. First of all, more than 3100 LSB-type units were directly spotted in Google Earth’s maps (<https://www.google.com/maps>) within 9 different Emilia-Romagna’s representative towns (*Carpi, Cento, Correggio, Crevalcore, Finale-Emilia, Mirandola, Reggiolo, San Felice sul Panaro* and *San Giovanni in Persiceto*), also confronting available 2D and 3D images; spotting the LSB-type buildings was possible because, in this part of the country, most of them are hosted outside the historical town centers, within well identifiable, special zones (explicitly called “industrial areas”). Secondly, population data was accessed from the website of the *Italian Statistical Institute*

(<http://www.istat.it>). The resulting LSB-buildings density curve—fitted with MATLAB’s *smoothingspline* (Mathworks 2017)—is shown in Fig. 16.

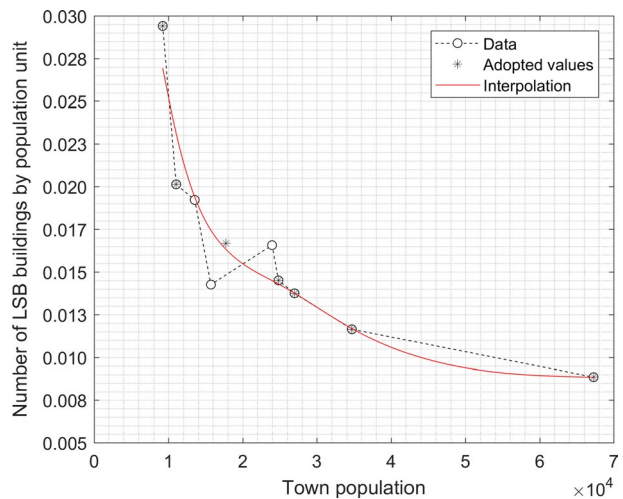
Using town population as an input, the grand total of LSB buildings is then estimated to be in the order of 16,753 units—with an average of circa 1.54 unit every 100 citizens. The reported buildings grand total takes into consideration structures to be used in agriculture, trade and industry. The geographical locations of all P0 elements were obtained—town by town—by randomly picking coordinates from actually known items, listed in the Emilia-Romagna’s database. We think such random selection can be considered a good approximation of the actual geographical positions as, by far, most of the structures are indeed located within small industrial areas.

6 Loss ratio frequency distribution function

As discussed in Sect. 5, the estimated total number of LSB buildings within the 54 towns is 16,753; the damaged ones (those listed in the database, with a damage pattern between P1 and P5) are 2083, or 12.4% of the total. With the available information, and by taking into account Γ and Ψ values (the latter distinguished by economic macrosector), it is possible to calculate an *empirical assessed loss ratio curve*. Such curve is given in Fig. 17; in it, on the X-axis, we report the frequency distribution of ξ (the so-called “Assessed Loss Ratio”), whose values were obtained by using Formula 4. In such formula, the denominator was assessed by business macrosector; this means that it does not provide specific information about the single building unit. As a consequence, loss ratios bigger than 1.0 may (and do) exist. Looking at Fig. 17, we notice that relative frequency distribution proves to be very close to an exponential function in the form $y = a \cdot \exp(b \cdot x)$ —with $a \approx 0.049$ and $b \approx -2.25$. In the figure, a black spot represents the undamaged buildings.

In Fig. 17, all the damage patterns from P1 to P5 are considered together, i.e. there is no distinction between the source of cost in terms of occurred damage level. To improve this, in Fig. 18 we show frequency distribution of ξ , disaggregated by damage pattern P_j , and represented in the semi-log space. Once the probability of incurring in a certain damage pattern (in a given time span) is known, such charts can be adopted in first-try assessment

Fig. 16 Density of LSB-type buildings by town population



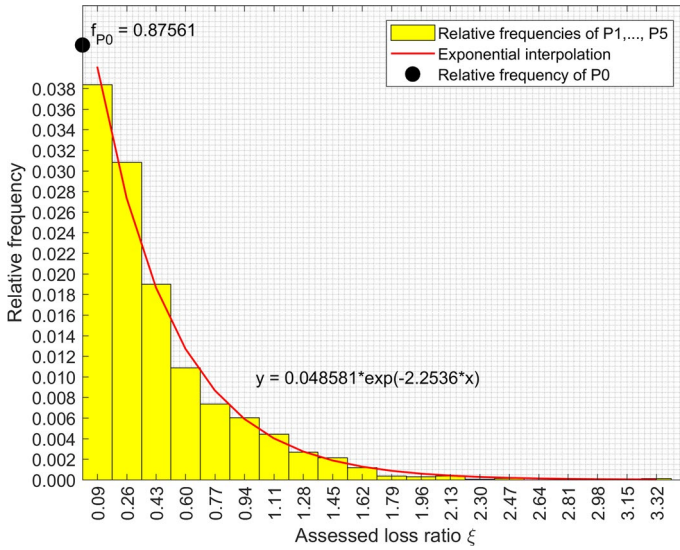


Fig. 17 Loss ratio frequency distribution function

of LSB buildings’ loss ratio. To this aim, in the charts we added fitting lognormal distributions, whose parameters are given in Table 5.

7 Empirical fragility functions

Once P0 items are computed for every one of the 54 towns, it becomes possible to define fragility functions (in terms of absolute probability, i.e. considering P0 among the possible outcomes). First of all, in Tables 6, 7, 8 and 9 we report damage matrixes we got from data analysis; the number of rows in the table was chosen so to enable the interested reader to make a comparison with the previously cited work of Buratti.

As a second step, data reported in the tables can be fitted with continuous curves. So far, the fragility evidences we showed just regarded counting the number of items per ground shaking bin (see Fig. 10 and Tables 6, 7, 8 and 9). Now, using Sum of Squares Errors (SSE) approach (Draper and Smith 1998), we show the fitting of the empirical results concerning PGA and PGV, with normal and logistic CDF functions respectively (ITL NIST 2012)—indeed, other ways are possible, e.g. (Buratti et al. 2017; Porter 2019). Here, the SSE approach consists of finding—for every damage pattern—the pair of parameters for which the induced error is minimum—see Formula 7.

$$\tilde{\mu}, \tilde{\sigma} = \arg \min_{\mu, \sigma} \sum_{i=1}^7 w_i \cdot \left(\frac{n_i}{b_i} - \Phi_{\mu, \sigma}(x) \right)^2 \tag{7}$$

where

- n_i is the number of items in the i th ground motion bin, whose damage pattern is equal or greater than the considered one;
- b_i is the total number of items in the i th ground motion bin;

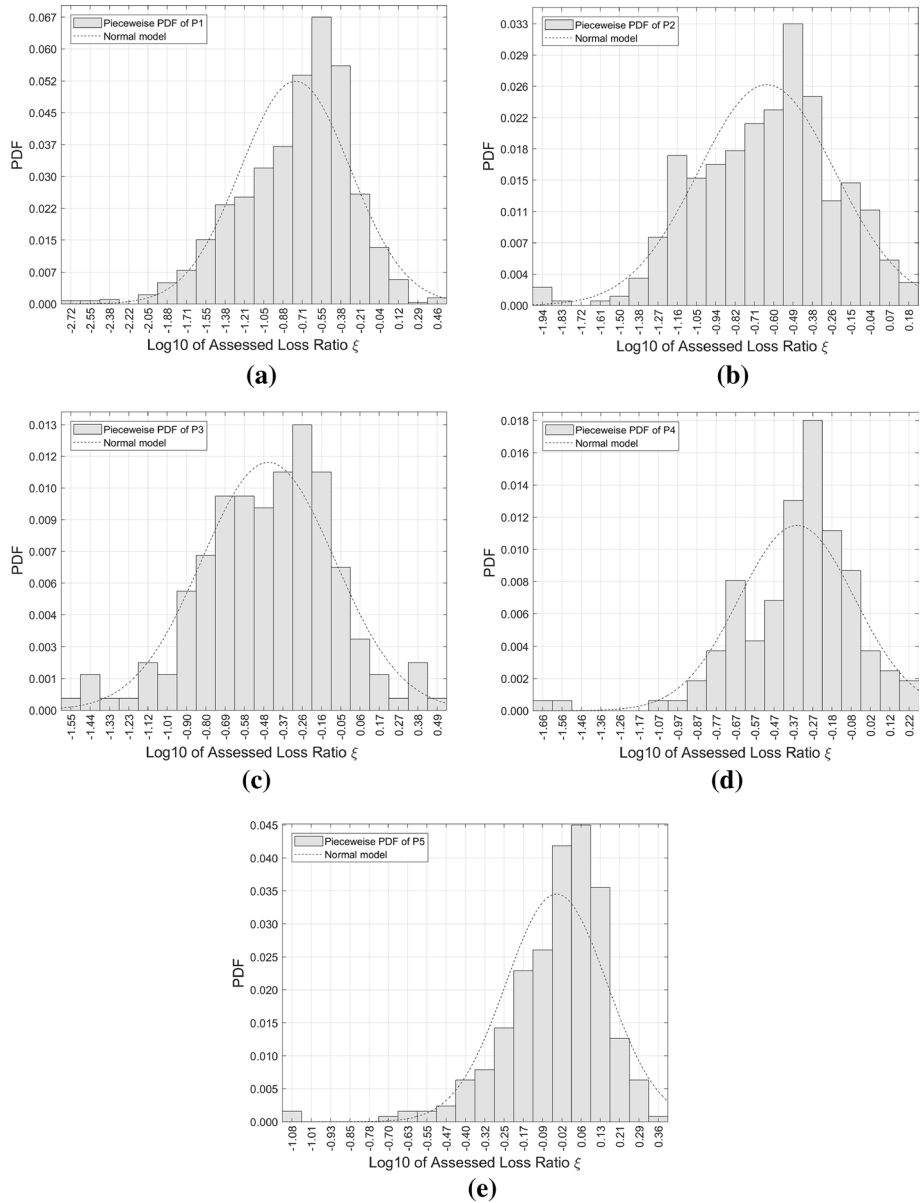


Fig. 18 Unconditioned Probability Density Functions for Log10 of assessed loss ratio values ξ , for damage patterns a P1, b P2, c P3, d P4 and e P5

Table 5 Values of characteristic parameters for the frequency distributions of ξ

	P1	P2	P3	P4	P5
μ	-0.77	-0.64	-0.45	-0.35	-0.04
σ	0.48	0.40	0.37	0.30	0.20

Table 6 Damage matrix for the whole set of LSB buildings: number of items per damage pattern, by PGA intervals (bins' span = 0.0504 g)

PGA (%g)	P0	P1	P2	P3	P4	P5	Tot
[0.00, 5.04]	3600	29	0	1	1	0	3631
[5.04, 10.09]	5052	222	19	4	0	6	5303
[10.09, 15.13]	1888	170	29	7	7	6	2107
[15.13, 20.17]	1502	168	35	14	13	19	1751
[20.17, 25.21]	1136	76	47	11	9	16	1295
[25.21, 30.26]	738	119	110	38	25	43	1073
[30.26, 35.3]	733	258	194	105	84	198	1572

Table 7 Cumulative damage matrix for the whole set of LSB buildings: relative number of items—by PGA intervals—equal or bigger than the considered damage pattern (bins' span = 0.0504 g)

PGA (%g)	P ≥ P0	P ≥ P1	P ≥ P2	P ≥ P3	P ≥ P4	P = P5
[0.00, 5.04]	1.000	0.009	0.001	0.001	0.000	0.000
[5.04, 10.09]	1.000	0.047	0.005	0.002	0.001	0.001
[10.09, 15.13]	1.000	0.104	0.023	0.009	0.006	0.003
[15.13, 20.17]	1.000	0.142	0.046	0.026	0.018	0.011
[20.17, 25.21]	1.000	0.123	0.064	0.028	0.019	0.012
[25.21, 30.26]	1.000	0.312	0.201	0.099	0.063	0.040
[30.26, 35.3]	1.000	0.534	0.370	0.246	0.179	0.126

Table 8 Damage matrix for the whole set of LSB buildings: number of items per damage pattern, by PGV intervals (bins' span = 10.193 cm/s)

PGV (cm/s)	P0	P1	P2	P3	P4	P5	Tot
[0.00, 10.19]	9364	303	25	7	2	6	9707
[10.19, 20.39]	2749	241	68	13	17	26	3114
[20.39, 30.58]	1088	127	45	16	11	14	1301
[30.58, 40.77]	468	63	54	14	14	24	637
[40.77, 50.96]	426	114	81	45	30	85	781
[50.96, 61.16]	403	158	132	72	47	107	919
[61.16, 71.35]	151	36	29	13	18	26	273

Table 9 Cumulative damage matrix for the whole set of LSB buildings: relative number of items—by PGV intervals—equal or bigger than the considered damage pattern (bins' span = 10.193 cm/s)

PGV (cm/s)	P ≥ P0	P ≥ P1	P ≥ P2	P ≥ P3	P ≥ P4	P = P5
[0.00, 10.19]	1.000	0.035	0.004	0.002	0.001	0.001
[10.19, 20.39]	1.000	0.117	0.040	0.018	0.014	0.008
[20.39, 30.58]	1.000	0.164	0.066	0.032	0.019	0.011
[30.58, 40.77]	1.000	0.265	0.166	0.082	0.060	0.038
[40.77, 50.96]	1.000	0.455	0.309	0.205	0.147	0.109
[50.96, 61.16]	1.000	0.561	0.390	0.246	0.168	0.116
[61.16, 71.35]	1.000	0.447	0.315	0.209	0.161	0.095

- w_i is the relative weight of the i th bin; as a first approach, weights are considered equally distributed;
- $\Phi_{\mu,\sigma}$ is the fitting CDF function (either normal or logistic).

The fitting problem was solved by iteration, both with reference to PGA and PGV; results are reported in Figs. 19 and 20; fitting parameters are given in Table 10.

The reader can check for the models' consistency by referring to Figs. 19f and 20f, that summarize this section's results. It has to be mentioned that the presented curves were obtained by interpolating fragility data points. This means that there is no direct empirical support for those curve sections beyond the maximum values of the intensity measures parameters, i.e. $PGA_{\max} = 0.353$ g and $PGV_{\max} = 71.35$ cm/s respectively.

For what concerns similar studies on the topic, the recent work (Buratti et al. 2017) has to be mentioned. In it, with reference to the Emilia-Romagna earthquake, fragility curves (in terms of PGA) that include five different damage patterns are presented; despite some similarities with our work exist, Buratti's results cannot be directly put in comparison to ours, for two main reasons (see also sub-Sect. 1.1 of this work): first of all, the team of Buratti accessed a smaller amount of data (just 923 damaged units, and 967 undamaged ones). Secondly, in the mentioned work, the reference building stock was assessed to have a total number of units between six and seven thousand; such estimation was done by taking cadastral data as a reference. On the contrary, we first determined an actual number of more than 3000 structures in just 9 towns, by directly counting them on a satellite map; then, we used an interpolation curve to assess the number of units in the remaining locations. Our bigger number of undamaged buildings leads to curves that, if compared to Buratti's, tend to rise at higher values of PGA. As said, this is partially due to a larger P0 stack, that makes the empirical data we have relatively less relevant. Among other works, in Palanci et al. (2017), fragility curves for precast industrial buildings are provided, in terms of PGV. Again, a direct comparison to our work is not possible, for many reasons (among which the different level of both seismic capacity and demand, as well as the fact that performance was assessed by running computer analyses); despite that, such work may serve in the future as a starting point for a case study application of our assessment tools. The main reference of the case study could be the expected reconstruction cost $E[\gamma]$ as presented in the next section.

8 Expected reconstruction cost

The here-presented fragility functions allow the reader to run consequence assessment analyses for LSB buildings, in socio-economic contexts that can be considered similar to that of Emilia-Romagna 2012. In particular, the convolution integral given in Formula 8 (as proposed in Rossi et al. 2019b), regarding the expected reconstruction cost $E[\gamma]$ within a given time span, can now be solved.

$$E[\gamma] = \sum_{i=1}^5 \left(\int_{\gamma_{\min}}^{\gamma_{\max}} \gamma \cdot f_{\gamma}(\gamma|P_i) d\gamma \cdot \int_{IM_{\min}}^{IM_{\max}} \mathcal{P}(P_i|IM) \cdot f(IM) \cdot dIM \right) \quad (8)$$

Indeed:

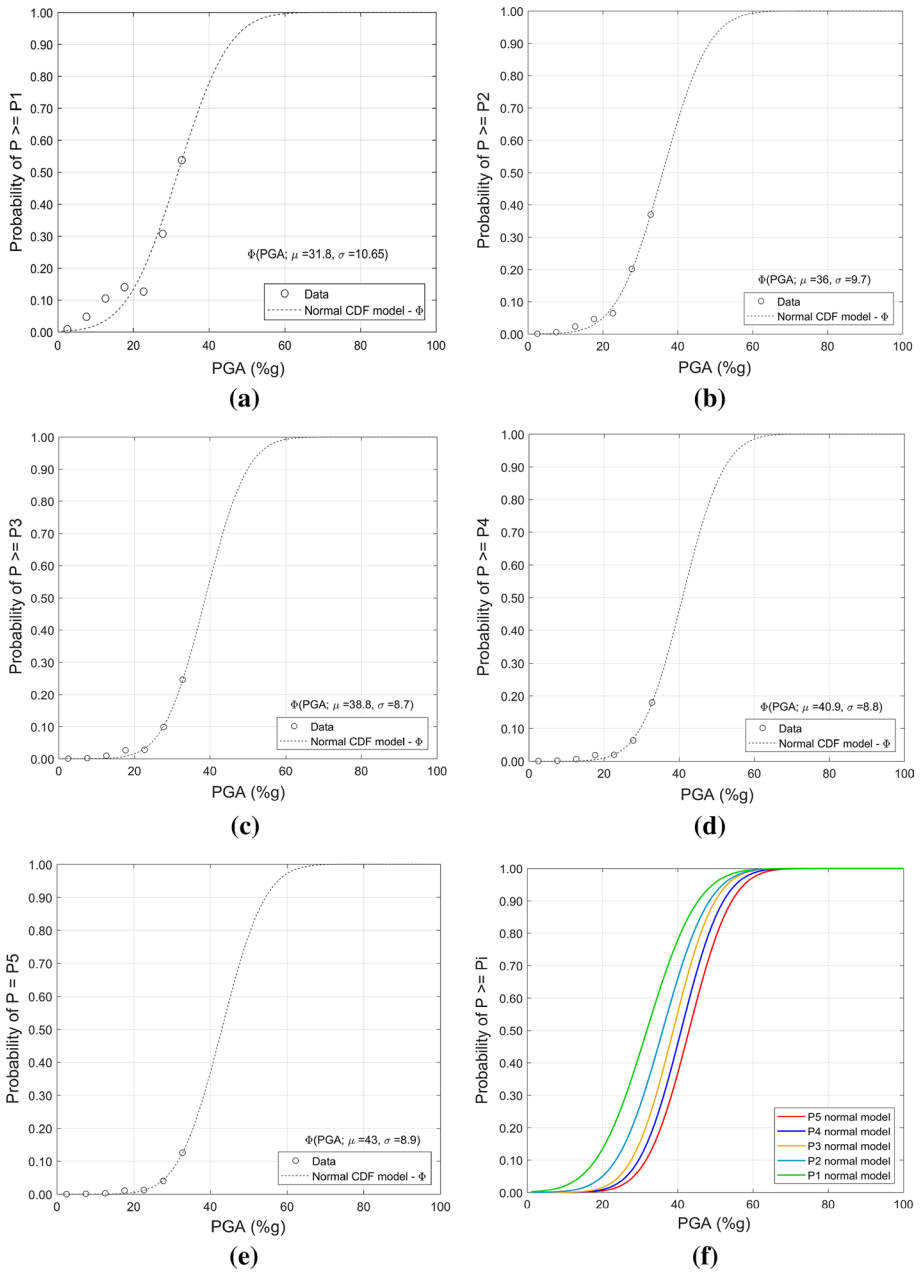


Fig. 19 Fitted normal CDFs to empirical set of damage data, in terms of PGA, by damage pattern **a** P1, **b** P2, **c** P3, **d** P4 and **e** P5, **f** all

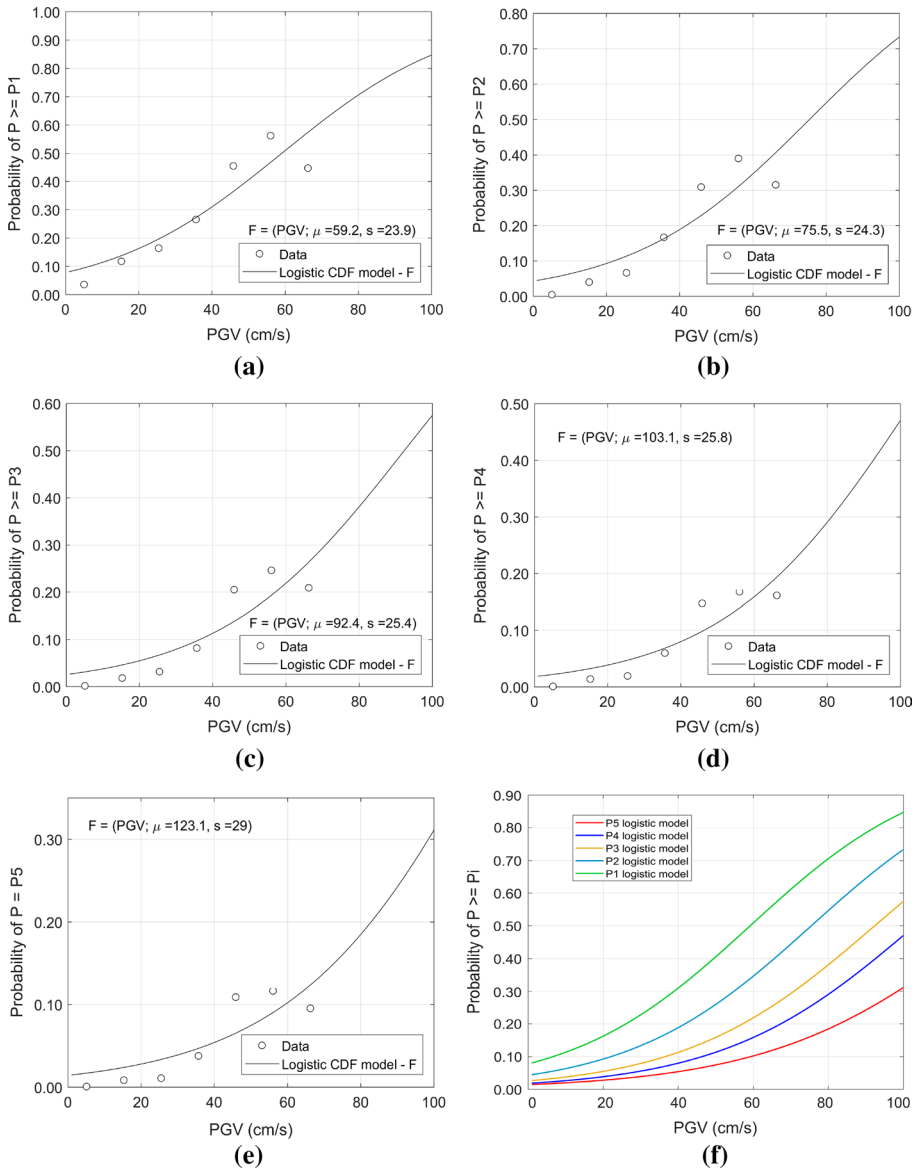


Fig. 20 Fitted logistic CDF to empirical set of damage data, in terms of PGV, for damage pattern **a** P1, **b** P2, **c** P3, **d** P4 and **e** P5, **f** all damage patterns

Table 10 Normal CDF fitting curves—PGA and PGV input

	P1	P2	P3	P4	P5
Normal (PGA, μ , σ)	(31.8, 10.6)	(36.0, 9.7)	(38.8, 8.7)	(40.9, 8.8)	(43.0, 8.9)
Logistic (PGV, μ , s)	(59.2, 23.9)	(75.5, 24.3)	(92.4, 25.4)	(103.1, 25.8)	(123.1, 29.0)

- f_γ is the probability density function of γ , defined for the i th damage pattern; this can be obtained from results presented in Rossi et al. (2019b).
- $\mathcal{P}(P_i|IM)$ is the probability of experiencing the i th damage pattern, once the intensity measure is known to be IM. This can be obtained from the empirical fragility curves we described in this text.
- $f(IM)$ is the probability density function of an intensity measure. Once the reference time span is known, this can be obtained from the site's hazard (see for example MIT 2008, 2018).

The practical solution of the integral, that is site-dependent, is deemed beyond the scope of this work. In a nutshell, data generated by the 2012 seismic event are modelled so to create innovative and portable assessment tools that can be used in practically solving the PBEE problem. Limitations exist, and are discussed in the next section.

9 Limitations and conclusions

After the 2012 Emilia-Romagna earthquake, a vast and consistent damage and loss database—so-called SFINGE—was created by the local public authority (Regione Emilia-Romagna), in order to fairly manage financial compensations to citizens and business owners. Interestingly, information was collected (among other things) with regard to structures' location, damage pattern and parametric direct economic losses. In this paper, we presented a research we have conducted on a subset of SFINGE database—i.e. the long-span-beams buildings dataset, or LSB—with the aim of developing data-based consequence assessment tools. First of all, a general description of the dataset, and of the underlying consequence classification rules, is given. As a second step, we presented empirical evidences about buildings' damage patterns spatial distribution; in this part, damage levels are put in relation with ground shaking intensity measures (as Peak Ground Acceleration, Modified Mercalli Intensity and Peak Ground Velocity); subsequently, we provided *conditioned* empirical fragility evidences, that serve as a reference for the fragility curves developed in the second part of the document. Then, the focus is put on economic consequence; in particular: (1) we provide cumulative distribution functions for both unitary loss and reconstruction cost; (2) we give useful charts regarding cumulative reconstruction cost, taking as independent variables the minimum distance from the epicenters, PGA, and PGV. From such charts, it clearly emerges that: (1) most of the consequence of the Emilia-Romagna earthquake happened in a near-fault region; (2) 50% of documented LSB-buildings' reconstruction cost (here indicated with the Greek symbol " Γ ") happens for $PGA \geq 28\%$ g; (3) Γ is almost linearly distributed in terms of PGV. So to make the obtained result more portable, we put economic consequences in terms of assessed loss ratio (ξ); this was done by evaluating the real-estate total value (Ψ) of each LSB building in the database. By doing this, it was possible to provide a discrete probability density distribution for ξ —that proved to be exponential. As a further step, we then introduced *unconditioned* empirical fragility functions. In this part, already presented fragility evidences are corrected, by introducing non-damaged building units from a second source of data. In the following section, cumulative distribution functions of normal distributions are fitted to the empirical curves, thus providing the reader with assessment tools that are both portable and comparable with existing literature. Being LSB-type buildings rather simple from the structural point of view, results' portability can be considered of great interest within seismic consequence

assessment procedures. As discussed in the text, the reported curves represent a considerable step forward if compared to the state of the art; the reason for this is that not only parametric direct economic losses are introduced for the first time, but also that the here considered set of information was cross-checked and validated by Regione Emilia-Romagna all along a 6-year programme for compensations distribution (funding application expired 30th June 2018). This guarantees that data are much more consistent, complete and reliable than ever before. In other words, the quality of information we used in this paper can be considered of the best level possible for the considered seismic scenario. As a final step, we discussed a convolution integral by which the expected reconstruction cost (in a given reference period) can be calculated; the solution is possible thanks to the assessment tools provided both in this paper and in the authors' previous works.

Limitations of reported results may arise mostly because of the way non-damaged structures (P0), that are essential to obtain the unconditioned fragility functions, were quantified and placed on the map. In any case, it has to be considered that, in Emilia-Romagna, most of the LSB buildings are located within special "industrial areas"—of usually limited extension—outside which only a small minority of LSB structures is likely to be found. Further research effort may help reducing uncertainty in the number and location of undamaged LSB buildings. Other limitations may regard the results portability: the data that form the backbone of this work were collected in a specific socio-economic context (that of Emilia-Romagna, in Northern Italy). Nonetheless, as already discussed by the authors in one introductory previous work (Rossi et al. 2019b), economic values may be translated in space and time using easily accessible correction parameters.

Further research may be dedicated to the numerical solution of the reported convolution integral, for practical loss assessment calculations of LSB structures.

Acknowledgements This research was supported by the European Commission with a Marie Skłodowska-Curie Individual Fellowship action (Project Data ESPerT—ID 743458, 2017/2019). We also thank the Italian public institution *Regione Emilia-Romagna*, and its *Struttura tecnica del Commissario delegato, Direzione generale economia della conoscenza, del lavoro e dell'impresa* and *Agenzia regionale per la ricostruzione—Sisma 2012*, who greatly assisted us during both the research process and the preparation of this manuscript.

Open Access This article is distributed under the terms of the Creative Commons Attribution 4.0 International License (<http://creativecommons.org/licenses/by/4.0/>), which permits unrestricted use, distribution, and reproduction in any medium, provided you give appropriate credit to the original author(s) and the source, provide a link to the Creative Commons license, and indicate if changes were made.

References

- ATC, Applied Technology Council (2012) Seismic performance assessment of buildings, FEMA P-58, volumes 1–3, <http://www.atccouncil.org>. Accessed 12 July 2019
- ARR, Agenzia regionale per la ricostruzione—Sisma 2012 (2018) *Analisi economica della ricostruzione degli edifici produttivi*. Centro Stampa Regione Emilia-Romagna, Bologna, p 145. ISBN 9788890737091 (in Italian)
- Aslani H (2005) Probabilistic earthquake loss estimation and loss disaggregation in buildings. Ph.D. Thesis, John A. Blume Earthquake Engineering Centre, Dept. of Civil and Environmental Engineering Stanford University, p 382
- Belleri A, Brunesi E, Nascimbene R, Pagani M, Riva P (2015) Seismic performance of precast industrial facilities following major earthquakes in the Italian territory. *J Perform Constr Facil.* [https://doi.org/10.1061/\(asce\)cf.1943-5509.0000617](https://doi.org/10.1061/(asce)cf.1943-5509.0000617)

- Bellotti C, Casotto C, Crowley H, Deyanova MG, Germagnoli F, Fianchisti G et al (2014) Single-storey precast buildings: probabilistic distribution of structural systems and subsystems from the sixties. *Progettazione Sismica* 5:41–70
- Bonfanti C, Carabellese A, Toniolo G (2008) Strutture prefabbricate: catalogo delle tipologie esistenti, RELUIS, Naples. <http://www.reluis.it>. Accessed 12 July 2019
- Bovo M, Savoia M (2019) Evaluation of force fluctuations induced by vertical seismic component on reinforced concrete precast structures. *Eng Struct* 178:70–87. <https://doi.org/10.1016/j.engstruct.2018.10.018>
- Buratti N, Minghini F, Ongaretto E, Savoia M, Tullini N (2017) Empirical seismic fragility for the precast RC industrial buildings damaged by the 2012 Emilia (Italy) earthquakes. *Earthq Eng Struct Dyn* 46:2317–2335
- Casotto C, Silva V, Crowley H, Nascimbene R, Pinho R (2015) Seismic fragility of Italian RC precast industrial structures. *Eng Struct* 94:122–136. <https://doi.org/10.1016/j.engstruct.2018.10.018>
- Cultrera G, Faenza L, Meletti C, D'Amico V, Michelini A, Amato A (2014) Shakemaps uncertainties and their effects in the post-seismic actions for the 2012 Emilia (Italy) earthquakes. *Bull Earthq Eng*. <https://doi.org/10.1007/s10518-013-9577-6>
- D'Aniello, M, La Manna Ambrosino G (2012) Terremoto dell'Emilia: report preliminare sui danni registrati a Bondeno (FE), Cento (FE), Finale Emilia (MO), San Prospero (MO) e Vigarano Mainarda (FE) in seguito agli eventi sismici del 20 e 29 maggio 2012. Rilievi e Verifiche di Agibilità dal 02 al 06 giugno 2012, RELUIS, Naples. <http://www.reluis.it>. Accessed 12 July 2019
- D'Ayala D, Spence R, Oliveira C, Pomonis A (1997) Earthquake loss estimation for Europe's historic town centres. *Earthq Spectra* 13(4):773–793
- Del Gaudio C, De Risi MT, Ricci P et al (2019) Empirical drift-fragility functions and loss estimation for infills in reinforced concrete frames under seismic loading. *Bull Earthq Eng* 17:1285. <https://doi.org/10.1007/s10518-018-0501-y>
- Draper NR, Smith H (1998) Applied regression analysis, 3rd edn. Wiley, Hoboken. ISBN 0-471-17082-8
- GEM Foundation (2018) OpenQuake. <https://www.globalquakemodel.org>. Accessed 12 July 2019
- Grünthal G (ed) (1998) European macroseismic scale 1998 (EMS-98). Centre Européen de Géodynamique et de Séismologie, Luxembourg
- GLASCI, Gruppo di Lavoro Agibilità Sismica dei Capannoni Industriali (2012) Linee di indirizzo per interventi locali e globali su edifici industriali mono-piano non progettati con criteri antisismici, RELUIS, Naples. <http://www.reluis.it>. Accessed 12 July 2019
- Hofer L, Zampieri P, Zanini MA, Faleschini F, Pellegrino C (2018) Seismic damage survey and empirical fragility curves for churches after the August 24, 2016 Central Italy earthquake. *Soil Dyn Earthq Eng* 111:98–109. <https://doi.org/10.1016/j.soildyn.2018.02.013>
- INGV, Istituto Nazionale di Geofisica e Vulcanologia (2012) <http://www.ingv.it/>. Accessed 12 July 2019
- INGV, Istituto Nazionale di Geofisica e Vulcanologia (2014) <http://cnt.rm.ingv.it/event/908231>. Accessed 12 July 2019
- ITL NIST—Information Technology Laboratory—National Institute of Technology (2012) Engineering statistics handbook. <https://www.itl.nist.gov/div898/handbook/>. Accessed 12 July 2019
- Lauciani V, Faenza L, Michelini A (2012) ShakeMaps during the Emilia sequence. *Ann Geophys* 55:4. <https://doi.org/10.4401/ag-6160>
- Liberatore L, Sorrentino L, Liberatore D, Decanini L (2013) Failure of industrial structures induced by the Emilia (Italy) 2012 earthquakes. *Eng Fail Anal* 34:629–647
- Lin L, Uma SR, King A (2016) Empirical fragility curves for non-residential buildings from the 2010–2011 Canterbury earthquake sequence. *J Earthq Eng*. <https://doi.org/10.1080/13632469.2016.1264322>
- Magliulo G, Ercolino M, Petrone C, Coppola O, Manfredi G (2014) The Emilia earthquake: seismic performance of precast reinforced concrete buildings. *Earthq Spectra* 30:891–912
- Mathworks (2017) MatLab R2017a, computer program. <http://www.mathworks.com>. Accessed 12 July 2019
- Minghini F, Ongaretto E, Ligabue V, Savoia M, Tullini N (2016) Observational failure analysis of precast buildings after 2012 Emilia earthquakes. *Earthq Struct* 11(2):327–346
- MIT, Ministero delle Infrastrutture e dei Trasporti (2008) Decreto Ministeriale del 14 gennaio 2008—Nuove Norme Tecniche per le Costruzioni, *Gazzetta Ufficiale* n. 29 (in Italian)
- MIT, Ministero delle Infrastrutture e dei Trasporti (2018) Decreto Ministeriale del 17 gennaio 2018—Aggiornamento delle “Norme Tecniche per le Costruzioni”, *Gazzetta Ufficiale* n. 8 del 20/02/2018 (in Italian)
- Miranda E, Aslani H (2003) Probabilistic response assessment for building-specific loss estimation, PEER. <https://peer.berkeley.edu>. Accessed 12 July 2019
- Nascimbene R, Brunesi E, Bolognini D, Bellotti D (2015) Experimental investigation of the cyclic response of reinforced precast concrete framed structures. *PCI J* 60(2):57–79. <https://doi.org/10.15554/pcij.03012.015.57.79>


- Palanci M, Senel S, Kalkan A (2017) Assessment of one story existing precast industrial buildings in Turkey based on fragility curves. *Bull Earthq Eng* 15(1):271–289
- Paolucci R, Mazzieri C, Smerzini C (2015) Anatomy of strong ground motion: near-source records and three-dimensional physics-based numerical simulations of the Mw 6.0 2012 May 29 Po Plain earthquake, Italy. *Geophys J Int* 203:2001–2020. <https://doi.org/10.1093/gji/ggv405>
- Parisi F, De Luca F, Petruzzelli F, De Risi R, Chioccarelli E, Iervolino I (2012) Field inspection after the May 20th and 29th 2012 Emilia-Romagna earthquakes. <http://www.reluis.it>. Accessed 12 July 2019
- Porter K (2019) A beginner's guide to fragility, vulnerability, and risk. University of Colorado Boulder, 119 pp. <http://spot.colorado.edu/~porterka/Porter-beginnersguide.pdf>. Accessed 12 July 2019
- Porter K, Kennedy R, Bachman R (2007) Creating fragility functions for performance-based earthquake engineering. *Earthq Spectra* 23(2):471–489. <https://doi.org/10.1193/1.2720892>
- Pres. R E-R, Presidente della Regione Emilia-Romagna in Qualità di Commissario Delegato (2012a) Linee Guida per la presentazione delle domande e le richieste di erogazione dei contributi previsti nell'Ordinanza N.57 e s.m.i. del 12 ottobre 2012 del Presidente in qualità di Commissario Delegato ai sensi dell'articolo 1, comma 2, del D.L. 74/2012 convertito con modificazioni. <https://www.regione.emilia-romagna.it>. Accessed 12 July 2019
- Pres. R E-R, Presidente della Regione Emilia-Romagna in Qualità di Commissario Delegato (2012b) TESTO COORDINATO Ordinanza n. 57 del 12 ottobre 2012 come modificata dall'Ordinanza n. 64 del 29 ottobre 2012 e dall'Ordinanza n. 74 del 15 novembre 2012. <https://www.regione.emilia-romagna.it>. Accessed 12 July 2019
- R E-R, Regione Emilia-Romagna (2012a) Elenco Regionale dei Prezzi delle Opere Pubbliche della Regione Emilia-Romagna—Art. 8 Legge Regionale N.11/2010—Art. 133 Decreto Legislativo 163/2006. <https://www.regione.emilia-romagna.it>. Accessed 12 July 2019
- R E-R, Regione Emilia-Romagna (2012b) SFINGE. <https://www.regione.emilia-romagna.it/terremoto/sfinge>. Accessed 12 July 2019
- R E-R, Regione Emilia-Romagna (2013) Prezzario Regionale per Opere e Interventi in Agricoltura Adeguateamento 2007. <https://www.regione.emilia-romagna.it>. Accessed 12 July 2019
- R E-R, Regione Emilia-Romagna (2018) 2012–2018 L'Emilia dopo il sisma—Report su sei anni di ricostruzione. <https://www.regione.emilia-romagna.it>. Accessed 12 July 2019
- Rossetto T et al (2012) The 20th May 2012 Emilia Romagna earthquake—EPICentre field observation report, UCL EPICentre. <http://www.ucl.ac.uk>. Accessed 12 July 2019
- Rossetto T, Iannou I, Grant DN (2013) Existing empirical fragility and vulnerability functions: compendium and guide for selection. GEM Technical Report 2013-X, GEM Foundation, Pavia, Italy, 2013. www.globallquakemodel.org. Accessed 12 July 2019
- Rossi L, Holtschoppen B, Butenweg C (2019a) Official data on the economic consequence of the 2012 Emilia-Romagna earthquake—a first analysis of database SFINGE. *Bull Earthq Eng* 17–9(2019):4855–4884. <https://doi.org/10.1007/s10518-019-00655-8>
- Rossi L, Parisi D, Casari C, Montanari L, Ruggieri G, Holtschoppen B, Butenweg C (2019b) Empirical data about direct economic consequences of Emilia-Romagna 2012 earthquake on long-span-beam buildings. *Earthq Spectra* 35(4):1979–2001. <https://doi.org/10.1193/100118eqs224dp>
- Rota M, Penna A, Strobbia CL (2008) Processing Italian damage data to derive typological fragility curves. *Soil Dyn Earthq Eng* 28(10–11):933–947
- Sabetta F, Goretti A, Lucantoni A (1998) Empirical fragility curves from damage surveys and estimated strong ground motion. In: Eleventh European conference on earthquake engineering, CD-ROM, ISBN: 90 5410 982 3, Balkema, January 1998
- Savoia M, Mazzotti C, Buratti N, Ferracuti B, Bovo M, Ligabue V et al (2012) Damages and collapses in industrial precast buildings after the Emilia earthquake. *Int J Earthq Eng* 29:120–131
- Savoia M, Buratti N, Vincenzi L (2017) Damage and collapses in industrial precast buildings after the 2012 Emilia earthquake. *Eng Struct* 137:162–180
- Scognamiglio L, Margheriti L, Mele F, Tinti E, Bono A, De Gori P, Lauciani V, Lucente FP, Mandiello AG, Marcocci C, Mazza S, Pintore S, Quintiliani M (2012) The 2012 pianura padana Emiliana seismic sequence: locations, moment tensors and magnitudes. *Ann Geophys* 55(4):549–559
- Sezen H, Whittaker AS (2006) Seismic performance of industrial facilities affected by the 1999 Turkey earthquake. *J Perform Constr Facil*. [https://doi.org/10.1061/\(ASCE\)0887-3828\(2006\)20:1\(28\)](https://doi.org/10.1061/(ASCE)0887-3828(2006)20:1(28))
- Syner-G Consortium (2013) SYNER-G: systemic seismic vulnerability and risk analysis for buildings, lifeline networks and infrastructures safety gain. European research project. <http://www.vce.at>. Accessed 12 July 2019
- Toniolo G, Colombo A (2012) Precast concrete structures: the lessons learned from the L'Aquila earthquake. *Struct Concr* 13:73–83
- USGS, United States Geological Survey (2012) <https://earthquake.usgs.gov/>. Accessed 20 October 2019

Wood HO, Neumann F (1931) Modified Mercalli Intensity Scale of 1931. *Seismol Soc Am Bull* 21(4):277–283

Yamaguchi N, Yamazaki F (2000) Fragility curves for buildings in Japan based on damage surveys after the 1995 Kobe earthquake. In: *Proceedings of the 12th world conference on earthquake engineering*, Auckland, New Zealand, January 30–February 4, 2000

Publisher's Note Springer Nature remains neutral with regard to jurisdictional claims in published maps and institutional affiliations.

Affiliations

Leonardo Rossi^{1,6}  · **Marco Stupazzini**² · **Davide Parisi**³ · **Britta Holtschoppen**⁴ · **Gabriella Ruggieri**³ · **Christoph Butenweg**⁵

¹ Lehrstuhl für Baustatik und Baudynamik (LBB), RWTH Aachen University, Mies-van-der-Rohe-Straße 1, 52074 Aachen, Germany

² Munich Re, Königinstraße 107, 80802 Munich, Germany

³ Agenzia Regionale per la Ricostruzione - Sisma 2012, Regione Emilia-Romagna, Viale Aldo Moro 52, 40127 Bologna, Italy

⁴ SDA-engineering Ingenieurgesellschaft mbH, Kaiserstraße 100, TPH III - B, 52134 Herzogenrath, Germany

⁵ Center for Wind and Earthquake Engineering (CWE), RWTH Aachen University, Mies-van-der-Rohe-Straße 1, 52074 Aachen, Germany

⁶ Department of Data Science and Knowledge Engineering (DKE), Maastricht University, P.O. 616, Maastricht 6200 MD, The Netherlands